The non-monotonicity of moist adiabatic warming

Osamu Miyawaki[a]

[a] *Department of Geosciences, Union College, Schenectady New York, USA*

Corresponding author: Osamu Miyawaki, miyawako@union.edu

ABSTRACT: The moist adiabat is a useful first-order approximation of the tropical stratification and thus governs fundamental properties of climate such as the static stability and the lapse rate feedback. While total atmospheric latent heating increases monotonically with warming, the resulting change in temperature along a moist adiabat is surprisingly non-monotonic with surface temperature. This phenomenon has lacked a physical explanation. This paper presents a thermodynamic explanation by decomposing the sensitivity of the moist adiabatic lapse rate into two competing components: 1) A Cooling Term arising from the partial derivative of saturation specific humidity with respect to temperature ($\partial q_s/\partial T$), which is proportional to q_s/T^2 via the Clausius-Clapeyron relation, and 2) a Pressure Term arising from the partial derivative with respect to pressure ($\partial q_s/\partial p$), which is proportional to q_s/p. The non-monotonicity arises because while both terms grow with temperature due to the exponential increase of saturation specific humidity (q_s), the $1/T^2$ prefactor on the Cooling Term suppresses its growth more strongly than the pressure-related prefactor on the Pressure Term. This mechanism also explains the non-monotonic behavior of convective buoyancy and vertical velocity.

1. Introduction

The Clausius-Clapeyron relation describes the potential for a warmer atmosphere to hold more water vapor (Emanuel 1994). This principle is the basis for the positive water vapor feedback (Held and Soden 2000) and various scaling theories in response to warming including extreme precipitation (O'Gorman 2015) and CAPE (Romps 2016).

In the tropics, convection couples the surface with the free troposphere. Although processes like convective entrainment influence the details of this coupling (Miyawaki et al. 2020), moist adiabatic adjustment serves as a useful first-order approximation (Held 1993). The top-heavy warming profile predicted by moist adiabatic adjustment (Fig. 1b) is a robust feature in climate models and observations, despite historical challenges in observational records (Vallis et al. 2015; Santer et al. 2005).

This warming profile is important because it increases atmospheric static stability, which influences convection (Neelin and Held 1987). This structure also defines the tropical lapse rate feedback, a key negative feedback for global climate sensitivity (Hansen et al. 1984). The lapse rate feedback partially cancels the water vapor feedback and scales in tandem because amplified warming in the upper troposphere is a consequence of enhanced latent heat release (Held and Shell 2012). In a moist adiabatic atmosphere that is saturated at the surface, total latent heat release $L_v(q_{\text{surface}} - q_{\text{top}})$ where q_{surface} is surface specific humidity and q_{top} is the cloud top specific humidity. For deep convection that reaches the tropopause we can approximate q_{top} as $q_{\text{tropopause}}$ where $q_{\text{tropopause}}$ is invariant with surface temperature (Seeley et al. 2019). Thus to first order we expect total latent heat release to scale as q_{surface}, which increases monotonically with surface temperature following the Clausius-Clapeyron relation (Fig. 1a).

Given the monotonic increase total latent heating with surface temperature, one might expect moist adiabatic warming to also increase monotonically with surface temperature at all levels. However, it is a non-monotonic function of surface temperature at fixed pressure levels (Fig. 1c, see Appendix A for details on how the moist adiabat is calculated). This non-monotonicity arises in height coordinates (Fig. A1), with or without latent heat of fusion (see Appendix B and Fig. B1), and across different empirical formula for saturation vapor pressure (see Appendix C and Fig. C1). While Levine and Boos (2016) showed this non-monotonicity and its influence on zonal stationary circulations, an explanation for the non-monotonicity in moist adiabatic warming does not exist in the literature.

This raises the question: What physical mechanism drives this non-monotonic warming? Here we provide a thermodynamic explanation for the origin of non-monotonicity in moist adiabatic warming and its cascading effects on buoyancy and vertical velocity.

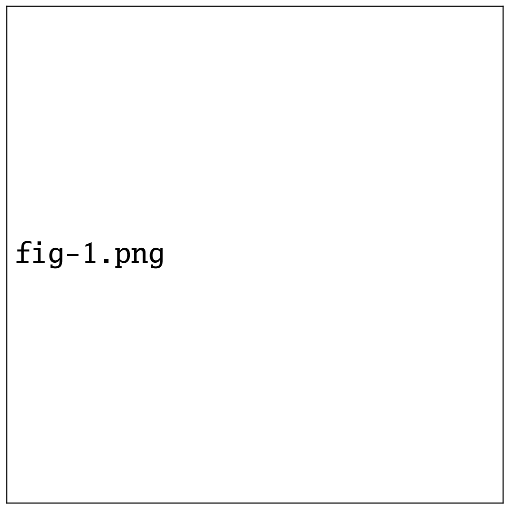

FIG. 1. (a) Surface saturation specific humidity increases monotonically with surface temperature. (b) Vertical profiles of moist adiabatic warming to a 4 K surface warming, plotted against pressure, for T_s = 280, 290, 300, 310, and 320 K. Warming decreases with surface temperature at lower levels while it increases with surface temperature at higher levels. (c) Moist adiabatic warming varies non-monotonically with surface temperature at all levels, e.g. at 500, 400, 300, and 200 hPa. Moist adiabatic warming peaks at warmer surface temperatures at higher levels.

2. Theory of Non-Monotonic Warming

We start by defining the moist adiabatic temperature profile in pressure coordinates $T(p)$ in terms of the moist adiabatic lapse rate $\Gamma_m = dT/dp$:

$$T(p) = T_s + \int_{p_s}^{p} \Gamma_m \, dp' \tag{1}$$

where T_s is surface temperature. The difference between a perturbed and baseline state (Δ) then follows as

$$\Delta T(p) = \Delta T_s + \int_{p_s}^{p} \Delta\Gamma_m \, dp' \tag{2}$$

For a small perturbation, $\Delta\Gamma_m$ can be approximated using a first-order Taylor expansion: $\Delta\Gamma_m \approx \frac{d\Gamma_m}{dT_s}\Delta T_s$. Substituting this into Eq. (2) gives:

$$\Delta T(p) \approx \Delta T_s + \left(\int_{p_s}^{p} \frac{d\Gamma_m}{dT_s} dp'\right) \Delta T_s \tag{3}$$

Thus the non-monotonicity in moist adiabatic warming is encoded into $d\Gamma_m/dT_s$, the sensitivity of the moist adiabatic lapse rate to surface temperature. Indeed, $d\Gamma_m/dT_s$ is non-monotonic with respect to temperature (dashed line shows the local minima of $d\Gamma_m/dT_s$ in Fig. 2a). Note that $d\Gamma_m/dT_s$ is mostly negative in the troposphere (Fig. 2b). This is consistent with amplified warming aloft because the integral in Eq. (2 is from high to low pressure, which introduces a negative sign.

Γ_m is a function of local state variables $\Gamma_m(T, p)$. Thus to make progress in understanding $d\Gamma_m/dT_s$, we must rewrite $d\Gamma_m/dT_s$ in terms of derivatives with respect to the local state variables (T, p). To do this we first use the chain rule:

$$\frac{d\Gamma_m}{dT_s} = \left(\frac{\partial\Gamma_m}{\partial T}\right)_p \cdot \frac{dT}{dT_s} + \left(\frac{\partial\Gamma_m}{\partial p}\right)_T \cdot \frac{dp}{dT_s} \tag{4}$$

The second term $\frac{dp}{dT_s} = 0$ because pressure is the vertical coordinate and is an independent variable. Recognizing that by definition $\Gamma_m = \frac{dT}{dp}$,

$$\frac{d}{dp}\left(\frac{dT}{dT_s}\right) = \left(\frac{\partial\Gamma_m}{\partial T}\right)_p \cdot \frac{dT}{dT_s} \tag{5}$$

This is an ordinary differential equation for $\frac{dT}{dT_s}$ as a function of pressure. The solution with the boundary condition $\frac{dT}{dT_s}(p_s) = 1$, is:

$$\frac{dT}{dT_s} = \exp\left(\int_{p_s}^{p} \left(\frac{\partial\Gamma_m}{\partial T}\right)_p dp'\right) \tag{6}$$

Substituting Eq. (6) back into Eq. (4) gives:

$$\frac{d\Gamma_m}{dT_s} = \left(\frac{\partial \Gamma_m}{\partial T}\right)_p \cdot \exp\left(\int_{p_s}^{p} \left(\frac{\partial \Gamma_m}{\partial T}\right)_{p'} dp'\right) \tag{7}$$

where $(\partial\Gamma_m/\partial T)_p$ is the moist adiabatic lapse rate sensitivity to local temperature T at pressure level p. The integral describes how a surface temperature perturbation influences Γ_m through the sum of all Γ_m changes that occur below p.

The non-monotonicity can arise from either 1) $(\partial\Gamma_m/\partial T)_p$ being non-monotonic and the integral acting to amplify it or 2) $(\partial\Gamma_m/\partial T)_p$ being monotonic but sign changes in $(\partial\Gamma_m/\partial T)_p$ leads to the integral being non-monotonic. Numerical solutions show that $(\partial\Gamma_m/\partial T)_p$ is non-monotonic (dash-dot line shows the local minima of $d\Gamma_m/dT$ in Fig. 2c), which is further amplified by the integral term (Fig. 2d).

Why is $(\partial\Gamma_m/\partial T)_p$ non-monotonic with T? To understand this we solve for Γ_m from the first law of thermodynamics for adiabatic ascent with latent heating assuming the parcel is saturated:

$$c_p dT - \alpha dp + L_v dq_s = 0 \tag{8}$$

where c_p is the specific heat capacity of air at constant pressure, α is specific volume, L_v is the latent heat of vaporization, and q_s is the saturation specific humidity. We assume 1) $c_p \approx c_{pd}$, neglecting the role of water of all phases on the specific heat capacity and 2) $\alpha \approx \alpha_d = R_d T/p$, neglecting the virtual effect of vapor on density.

Use the chain rule to expand dq_s:

$$dq_s = \left(\frac{\partial q_s}{\partial T}\right)_p dT + \left(\frac{\partial q_s}{\partial p}\right)_T dp \tag{9}$$

Substituting Eq. (9) into Eq. (8) and rearranging gives

$$\left(c_{pd} + L_v \left(\frac{\partial q_s}{\partial T}\right)_p\right) dT = \left(\alpha_d - L_v \left(\frac{\partial q_s}{\partial p}\right)_T\right) dp \tag{10}$$

We can derive closed-form expressions for the q_s derivatives using the Clausius-Clapeyron relation and Dalton's Law. These q_s derivatives describe the role of phase equilibrium shifts in q_s with T

and p on the effective heat capacity and specific volume of the air parcel, respectively:

$$c_L \equiv L_v \left(\frac{\partial q_s}{\partial T}\right)_p \approx \frac{L_v^2 q_s}{R_v T^2} \tag{11}$$

$$\alpha_L \equiv -L_v \left(\frac{\partial q_s}{\partial p}\right)_T \approx \frac{L_v q_s}{p} \tag{12}$$

where the approximation arises from assuming saturation vapor pressure $e_s \ll p$.

c_L can be thought of as a latent heat capacity, representing the enhanced thermal inertia due to the fact that latent heating buffers some of the cooling from expansion. Thus c_L acts to increase the heat capacity of the air parcel such that it has an effective heat capacity $c_{pd} + c_L$.

α_L can be thought of as a latent specific volume, representing the enhanced expansion of air with ascent due to the fact that lower pressure shifts the phase equilibrium of water to favor the vapor phase over liquid. Thus α_L acts to increase the volume of air such that it has an effective specific volume $\alpha_d + \alpha_L$.

Now solving for the moist adiabatic lapse rate $\Gamma_m = dT/dp$:

$$\Gamma_m = \frac{dT}{dp} = \frac{\alpha_d + \alpha_L}{c_{pd} + c_L} \tag{13}$$

$$= \Gamma_d \cdot \frac{1 + \frac{\alpha_L}{\alpha_d}}{1 + \frac{c_L}{c_{pd}}} \tag{14}$$

where $\Gamma_d = \alpha_d / c_{pd}$ is the dry adiabatic lapse rate in pressure coordinates and the two non-dimensional terms represent the fractional increase in effective heat capacity and specific volume due to phase equilibrium changes:

$$\tilde{c} = \frac{c_L}{c_{pd}} = \frac{L_v^2 q_s}{c_{pd} R_v T^2} \tag{15}$$

$$\tilde{\alpha} = \frac{\alpha_L}{\alpha_d} = \frac{L_v q_s}{R_d T} = \frac{R_v c_{pd} T}{R_d L_v} \tilde{c} = k\tilde{c} \tag{16}$$

Substituting Eq. (15) and Eq. (16) into Eq. (14) gives:

$$\Gamma_m = \Gamma_d \cdot \frac{1 + k\tilde{c}}{1 + \tilde{c}} \tag{17}$$

For typical values in Earth's atmosphere ($R_v = 461$ J kg^{-1} K^{-1}, $R_d = 287$ J kg^{-1} K^{-1}, $c_{pd} = 1005$ J kg^{-1} K^{-1}, $L_v = 2.5 \times 10^6$ J kg^{-1}, and $T \in [200, 320]$ K), the factor $k = \frac{R_v c_{pd} T}{R_d L_v} \in [0.13, 0.21]$. Thus k is a weak function of temperature and is a quasi-constant of order 10^{-1}. In contrast, $\tilde{c}$ scales exponentially with temperature (through q_s) and varies from $\tilde{c}(200\text{ K}) \sim 10^{-4}$ to $\tilde{c}(320\text{ K}) \sim 10^{1}$. Thus the temperature sensitivity of Γ_m is controlled by $\tilde{c}$. Because Γ_m is bounded between Γ_d (dry limit, $\tilde{c} \to 0$) and $k\Gamma_d$ (moist limit, $\tilde{c} \to \infty$), the magnitude of $\partial\Gamma_m/\partial T$ must peak at some intermediate $\tilde{c}$ else Γ_m would be unbounded.

Where does the magnitude of $\partial\Gamma_m/\partial T$ reach its peak value? To solve this we use the quotient rule on Eq. (13):

$$\frac{\partial\Gamma_m}{\partial T} = \underbrace{\frac{1}{c_{pd}+c_L}\frac{\partial(\alpha_d+\alpha_L)}{\partial T}}_{\text{latent volume sensitivity}} + \underbrace{\left(-\frac{\alpha_d+\alpha_L}{(c_{pd}+c_L)^2}\frac{\partial c_L}{\partial T}\right)}_{\text{latent heat capacity sensitivity}} \tag{18}$$

The latent volume sensitivity varies monotonically with T_s (Fig. 3a, c). The latent heat capacity sensitivity varies non-monotonically with T_s (Fig. 3b, d). Thus we further decompose the latent heat capacity sensitivity to probe its origin:

$$-\frac{\alpha_d+\alpha_L}{(c_{pd}+c_L)^2}\frac{\partial c_L}{\partial T} = -\frac{1}{p}\cdot(1+\tilde{\alpha})\cdot\frac{R_d}{c_{pd}}\frac{\partial\log c_L}{\partial\log T}\cdot f_d\cdot f_L \tag{19}$$

where

$$f_d \equiv c_d/(c_{pd}+c_L) \tag{20}$$

$$f_L \equiv c_L/(c_{pd}+c_L) \tag{21}$$

and $f_d + f_L = 1$. f_d and f_L represent the dry and latent fractions of effective heat capacity.

Eq. (19) shows the latent heat capacity sensitivity is a product of four terms that vary monotonically with T. $\tilde{\alpha} = L_v q_s/(\alpha_d p)$ scales exponentially with T through q_s (red line in Fig. 4a). The fractional change in latent heat capacity to a fractional change in temperature $\partial\log c_L/\partial\log T = L_v/(R_v T) - 2$ so it weakly decreases with T (blue line in Fig. 4a). The product of these two terms is weakly non-monotonic in T with a local minimum where $\tilde{\alpha} \approx R_v T/L_v$ (white line in Fig. 4b). At low T, $\tilde{\alpha}$ is small so the product is dominated by the decrease in $\partial\log c_L/\partial\log T$. At high T, $\tilde{\alpha}$ is large so the product is dominated by the exponential increase in $\tilde{\alpha}$. However, the non-monotonicity of these two terms are not the source of the peak in the magnitude of $\partial\Gamma_m/\partial T$, which requires a local maximum, not a minimum.

The dry fraction of effective heat capacity $f_d = c_{pd}/(c_{pd} + c_L)$ logistically decreases with T because c_{pd} is a constant while latent heat capacity c_L increases exponentially with T through q_s (blue line in Fig. 4c). The latent fraction of effective heat capacity $f_L = c_L/(c_{pd} + c_L)$ logistically increases with T (red line in Fig. 4c). The product $f_d \cdot f_L$ is maximized when $f_d = f_L$, or $c_L = c_{pd}$ (black line in Fig. 4d).

What is the physical intuition behind the peak at $c_L = c_{pd}$? Recall that c_L quantifies the enhancement of effective heat capacity due to latent heat of condensation offsetting adiabatic cooling. The q_s derivative in c_L requires two ingredients: 1) cooling from expansion and 2) water vapor. f_d and f_L represent the fractional availability of the two ingredients. At low T, condensation is limited by the availability of water vapor (red line in Fig. 4c). At high T condensation is limited by adiabatic cooling (blue line in Fig. 4c). The peak in latent heat capacity sensitivity corresponds to where the availability of cooling and vapor are equally limiting (black line in Fig. 4c). Thus the non-monotonicity in $\partial\Gamma_m/\partial T$ and moist adiabatic warming arises from the competition between the two limiting factors of condensation.

How well does the condition $c_L = c_{pd}$ capture the actual peak in $\partial\Gamma_m/\partial T$? The theory slightly overpredicts the T_s where the magnitude of $\partial\Gamma_m/\partial T$ peaks (compare solid and dash-dot lines in Fig. 5). This error is due to the weak non-monotonicity in the product $(1 + \tilde{\alpha})R_d/c_{pd}\partial \log(c_L)/\partial \log(T)$ which decreases with pressure (Fig. 4b). The error maximizes at the surface where the theory predicts a peak T_s that is 1.6 K warmer than the true peak T_s.

The error in T_s predicted by the theory and the true peak of Γ_m/dT_s grows with height because the integral term in Eq. (7) amplifies the error in $\partial\Gamma_m/\partial T$ at each level below. This error maximizes at 420 hPa where $c_L = c_{pd}$ predicts a peak T_s that is 2.0 K warmer than the true peak T_s (compare solid and dashed lines in Fig. 5). This error is further compounded for T_s corresponding to the peak of moist adiabatic warming ΔT (Eq. 3), leading to a maximum error of 6.6 K at 420 hPa (compare solid and dotted lines in Fig. 5). Thus the condition $c_L = c_{pd}$ provides a useful first-order estimate of T_s where moist adiabatic warming peaks. Importantly the theory successfully captures the shift to warmer peak T_s with height, which is due to the fact that temperature decreases with height and thus the transition from the vapor limited to cooling limited regime occurs at a warmer surface temperature with height.

3. Implications of non-monotonicity in moist adiabatic warming on convection

The non-monotonic warming of a moist adiabat has implications for the dynamics of convection. For example, Romps (2016) showed that parcel buoyancy is a non-monotonic function of surface temperature. Specifically the criterion where B peaks is $\beta = 2c_{pd}$ where

$$\beta = c_{pd} + L_v \frac{\partial q_s}{\partial T} = c_{pd} + c_L \tag{22}$$

Thus the criterion that maximizes B is equivalent to where moist adiabatic warming peaks, $c_{pd} = c_L$. Below, we show this is true if the entrainment parameter $a = PE\epsilon/g$[1] is small and derive a more general criterion that maximizes B.

Buoyancy B is the normalized virtual temperature (or equivalently, density) difference between the rising parcel $T_{v,p}$ and the environment $T_{v,e}$. Here we neglect the virtual effects of water and we use standard temperature:

$$B \approx \frac{g}{T_e}(T_p - T_e) \tag{23}$$

As before, we express temperature profiles in terms of T_s and the integral of their respective lapse rates. We assume the parcel follows a moist adiabatic lapse rate, Γ_m, while the environment follows an entraining lapse rate, Γ_e.

$$T_p = T_s + \int_{p_s}^{p} \Gamma_m(p')\, dp' \tag{24}$$

$$T_e = T_s + \int_{p_s}^{p} \Gamma_e(p')\, dp' \tag{25}$$

Substituting Eq. (24) and (25) into the definition of buoyancy Eq. (23) yields:

$$B \approx \frac{g}{T_e} \int_{p_s}^{p} \delta\Gamma\, dp' \tag{26}$$

[1] PE is precipitation efficiency, ϵ is the fractional entrainment rate, and g is gravitational acceleration. See Romps (2016) for the derivation of the entraining plume model.

fig-2.png

Fig. 2. (a) The sensitivity of the moist adiabatic lapse rate to surface temperature, $d\Gamma_m/dT_s$, varies non-monotonically with surface temperature. (b) $d\Gamma_m/dT_s$ has a local minimum across surface temperature at all pressure levels, e.g. across 500, 400, 300, and 200 hPa. A minimum in $d\Gamma_m/dT_s$ corresponds to a maximum in moist adiabatic warming (Fig. 1b) because the integral bounds in Eq. 3 decreases from p_s to p, which introduces a negative sign. The local minimum shifts toward warmer with surface temperature at higher levels. (c) The sensitivity of the moist adiabatic lapse rate to the local temperature at pressure p, $\partial\Gamma_m/\partial T$, also varies non-monotonically with surface temperature. (d) The integral term in Eq. (7) amplifies the non-monotonicity of $\partial\Gamma_m/\partial T$. (a) is the product of (c) and (d).

fig-3.png

FIG. 3. The moist adiabatic lapse rate sensivity to local temperature T, $\partial\Gamma_d/\partial T$ (Fig. 2c), is decomposed into contributions from (a) the latent volume sensivity and (b) the latent heat capacity sensitivity following Eq. (18). (c) The latent volume sensitivity monotonically increases increases with local temperature T across all pressure levels, e.g. across 500, 400, 300, and 200 hPa. (d) The latent heat capacity sensitivity has a local minimum that shifts toward warmer surface temperature at higher levels, consistent with the behavior of $d\Gamma_d/dT_s$ (Fig. 2b).

where $\delta\Gamma = \Gamma_e - \Gamma_m$. We use the same entraining plume model as in Romps (2016) but express the lapse rate in pressure coordinates:

$$\Gamma_e = \Gamma_d \cdot \frac{(1+a)\alpha_d + \alpha_L}{(1+a)c_{pd} + c_L} \tag{27}$$

fig-4.png

FIG. 4. The latent volume sensitivity is decomposed into a product of four terms (Eq. 19) that varies monotonically with local temperature T, where local means at pressure p. (a) The latent volume ratio $\tilde{\alpha}$ increases exponentially with local temperature (red line) while the fractional change in latent heat capacity c_L to a fractional change in local temperature T decreases linearly with T (blue line). The product of the two is weakly non-monotonic with T where the product has a local minimum (purple line). (b) The local minimum approximately occurs where $\tilde{\alpha} = R_v T / L_v$ (white line). (c) The latent heat capacity fraction f_L increases logistically with local temperature T (red line) while the dry heat capacity fraction f_d decreases logistically with T (blue line). The product of the two is non-monotonic with T where the product has a local maximum (purple line). (d) The local maximum occurs where $c_L = c_{pd}$ (black line).

Substituting Eq. (13) and (27) into Eq. (26) and simplifying gives:

$$B = \frac{g}{T_e} \int_{p_s}^{p} \Gamma_d \cdot \frac{a(1-k)\tilde{c}}{(1+a+\tilde{c})(1+\tilde{c})} \, dp' \tag{28}$$

If we assume that a does not vary with T_s, T_e increases monotonically with T_s at all p. The origin of the non-monotonicity of B must be in the integrand, $\delta\Gamma$. B depends on T primarily through $\tilde{c}$, which scales exponentially with T through q_s, whereas Γ_d and k are linear functions of T. In the limit of $\tilde{c} \longrightarrow 0$ (cold and dry), $\delta\Gamma$ scales as $\tilde{c}$, which increases with T. In the limit of $\tilde{c} \longrightarrow \infty$ (warm and humid), $\delta\Gamma$ scales as $\tilde{c}^{-1}$, which decreases with increasing T. Thus the integrand maximizes at some intermediate $\tilde{c}$.

To solve for the condition that maximizes buoyancy we solve for the $\tilde{c}$ derivative of the integrand $\delta\Gamma$ in Eq. (28) and set it to zero:

$$\frac{d}{d\tilde{c}} \left(\Gamma_d \cdot \frac{a(1-k)\tilde{c}}{(1+a+\tilde{c})(1+\tilde{c})} \right) = 0 \tag{29}$$

If we assume that a, k, and Γ_d do not vary with T, the solution to Eq. (29) is

$$\tilde{c}_{\text{peak}} = \sqrt{1+a} \tag{30}$$

Thus the condition that maximizes buoyancy is $c_L = \sqrt{1+a}c_{pd}$. In the limit of weak entrainment $a \longrightarrow 0$, this reduces to $c_L = c_{pd}$. In the presence of entrainment, buoyancy peaks at a higher c_L and thus higher T_s all else equal. Entrainment reduces the latent heat released by the cooling parcel given the same q_s so it shifts the critical point that separates the vapor limited and cooling limited regimes toward higher q_s.

How important is the factor $\sqrt{1+a}$? For an entrainment rate representative of Earth's current climate $a = 0.2$, the difference in peak T_s that corresponds to $c_L = c_{pd}$ and $c_L = \sqrt{1+a}c_{pd}$ are < 1.49 K (compare red and solid black line in Fig. 6a). This difference decreases with height and becomes negligibly small around the tropopause (e.g., 0.33 K at $p = 100$ hPa), which explains why the criteria $c_L = c_{pd}$ works well for explaining the non-monotonicity of CAPE (Romps 2016). However, for stronger entrainment rates and for understanding the non-monotonicity of buoyancy in the lower troposphere the factor $\sqrt{1+a}$ can be important (e.g., 4.38 K for $a = 0.7$ at the surface; compare red and solid black line in Fig. 6b).

How well do these criteria capture the T_s that maximizes buoyancy across the troposphere? We will first focus on $\delta\Gamma$, i.e. the integrand in Eq. (26). For $a = 0.2$ both criteria capture the T_s that corresponds to the peak in $\delta\Gamma$ well (< 1.39 K for $c_L = \sqrt{1+a}c_{pd}$, < 2.87 K for $c_L = c_{pd}$, compare red and solid black line to dashed line in Fig. 6a). The small error arises even for the $c_L = \sqrt{1+a}c_{pd}$ criterion because $\Gamma_d(1-k)$ is weakly non-monotonic with T (Γ_d increases with T and $(1-k)$ decreases with T), which we ignored in order to analytically solve Eq. (29). This error is amplified as we integrate $\delta\Gamma$ to obtain buoyancy Eq. (26) because the errors in the location of peak $\delta\Gamma$ from each level below accumulates for the location of peak B compare red and solid black line to dotted line in Fig. 6a).

For a higher entrainment parameter $a = 0.7$ the importance of the factor $\sqrt{1+a}$ becomes clear. The error in T_s that corresponds to the peak in $\delta\Gamma$ is < 3.39 K for the $c_L = \sqrt{1+a}c_{pd}$ criterion compared to < 5.83 K for the $c_L = c_{pd}$ criterion (compare red and solid black line to dashed line in Fig. 6b). The error in T_s that corresponds to the peak in buoyancy is surprisingly lower for the $c_L = c_{pd}$ criterion (< 3.37 K) compared to the $c_L = \sqrt{1+a}c_{pd}$ criterion (< 4.66 K, compare red and solid black lines to dotted black line in Fig. 6b). This is because $c_L = c_{pd}$ underpredicts T_s for peak B in the lower troposphere, which offsets the growth of the larger error in peak $\delta\Gamma$ (compare solid black and dotted lines in Fig. 6b). While the criteria $c_L = c_{pd}$ may provide a better estimate of peak buoyancy in some cases, it doesn't do so for the right reasons. For example the criteria $c_L = c_{pd}$ predicts no shift in T_s that maximizes B to perturbations in a while the criterion $c_L = \sqrt{1+a}c_{pd}$ captures the shift in peak $\delta\Gamma$ and B toward warmer T_s with increasing entrainment (Fig. 6c).

This non-monotonic behavior of buoyancy extends to the strength of the convective updraft. We model the updraft's specific kinetic energy, $\frac{1}{2}w^2$, using Eq. (1) from Del Genio et al. (2007):

$$\frac{d}{dz}\left(\frac{1}{2}w^2\right) = a'B(z) - (1+b')\epsilon(z)w^2 \tag{31}$$

where a' and b' are dimensionless constants. We use $a' = 1/6$ and $b' = 2/3$ following Del Genio et al. (2007). $\epsilon(z)$ is the fractional entrainment rate, which is calculated following Eq. (3) in Romps

(2016) with entrainment parameter $a = 0.2$ and precipitation efficiency $PE = 0.35$. Since $w(z)$ is determined by the integral of the net force, which includes buoyancy, we expect the non-monotonic dependence on T_s extends to the vertical velocity profile as well.

Numerically integrating Eq. (31) confirms this expectation. The resulting vertical velocity varies non-monotonically with T_s (Fig. 7b). This leads w(z) becoming more top-heavy with warming, i.e. w decreases in the lower troposphere and increases in the upper troposphere (Fig. 7a).

Are these findings relevant to Earth's atmosphere, where convection is not strictly moist adiabatic and vertical velocity is subject to details and constraints not considered here such as cloud microphysics and radiative cooling? To test this we analyzed output from a set of 9 convective-resolving models simulating radiative convective equilibrium in a 100 km x 100 km domain from the RCEMIP project (Wing et al. 2018). We look at the mean vertical velocity profiles for w exceeding the 99.9th percentile at each height level. The 99.9th percentile corresponds to the fastest 1000 samples of w per level per model. We focus on strong convective updrafts because the buoyancy is highest for those parcels that are closest to the moist adiabat.

The vertical velocity profiles from the RCEMIP simulations show diverse $w_{>99.9}$ responses to variations in surface temperature (295, 300, and 305 K, see Fig. 8). Some models exhibit a clear top-heavy shift in $w_{>99.9}$ with warming (e.g., CM1, DAM, UCLA-CRM, UKMO, WRF) accompanied by a decrease in $w_{>99.9}$ in the lower troposphere that is qualitatively consistent with the moist adiabatic theory (Fig. 7a). SAM shows a top-heavy shift in $w_{>99.9}$ without a clear decrease in $w_{>99.9}$ in the lower troposphere. In the remaining models the $w_{>99.9}$ response exhibits non-monotonicity with T_s but the peak $w_{>99.9}$ does not necessarily increase. For example DALES and SCALE predict a non-monotonic response in $w_{>99.9}$ with T_s at $z \approx 8$ km but the peak $w_{>99.9}$ weakens from $T_s = 300$ to 305 K. MesoNH also predicts a decrease in peak $w_{>99.9}$ from $T_s = 300$ K to 305 K but predicts a non-monotonic response in $w_{>99.9}$ with T_s at $z \approx 3$ km, much lower than in DALES and SCALE. The diversity in responses likely arises from differences in model details and emergent behavior such as convective organization that influence convective dynamics beyond the thermodynamic processes considered here. Nonetheless, the presence of non-monotonicity and a top-heavy shift in several models suggest that the implications of non-monotonicity in moist adiabatic warming on convective dynamics may be playing a role in shaping the response of convective updrafts in the real atmosphere.

fig-5.png

Fig. 5. Surface temperature T_s corresponding to the criteria $c_L = c_{pd}$ (solid), the minimum of the moist adiabatic lapse rate sensitivity to local temperature $\partial\Gamma_m/\partial T$ (dash dot), the minimum of the moist adiabatic lapse rate sensitivity to surface temperature $d\Gamma_m/dT_s$ (dashed), and the maximum of moist adiabatic warming ΔT (dotted). The theory most accurately captures the T_s corresponding to the minimum of $\partial\Gamma_m/\partial T$. The discrepancy between the theory and the T_s corresponding to the minimum of $d\Gamma_m/dT_s$ and ΔT are larger because the error at pressure p is the accumulation of errors at levels below p (see Eq. 7 and 3).

fig-6.png

Fig. 6. Surface temperature T_s corresponding to the criterion $c_L = c_{pd}$ (solid black), the criterion $c_L = c_{pd}\sqrt{1+a}$ (red), the maximum of buoyancy B (dotted), and the minimum of the difference between an entraining lapse rate and moist adiabatic lapse rate $\delta\Gamma = \Gamma_e - \Gamma_m$ (dashed) for the entrainment parameter (a) $a = 0.2$ and (b) $a = 0.7$. (c) The criterion $c_L = c_{pd}\sqrt{1+a}$ captures the a dependence of $\delta\Gamma$ and B extrema evaluated at pressure $p = 500$ hPa. In comparison the criterion $c_L = c_{pd}$ is not sensitive to the entrainment parameter a (vertical black line).

fig-7.png

Fig. 7. (a) Vertical profiles of vertical velocity, calculated by numerically integrating Eq. (31) in height using buoyancy B from Eq. (23). Vertical velocity decreases with surface temperature at lower levels while it increases with surface temperature at higher levels. (b) Vertical velocity varies non-monotonically with surface temperature at all levels, e.g. at 5, 10, 15, and 20 km. Vertical velocity peaks at warmer surface temperatures at higher levels consistent with the behavior of buoyancy (Fig. 6a) and moist adiabatic warming (Fig. 5).

fig-8.png

Fig. 8. Updraft velocity from 9 cloud resolving models (CM1, DALES, DAM, MesoNH, SAM-CRM, SCALE, UCLA-CRM, UKMO-CASIM, and WRF) that participated in RCEMIP (Wing et al. 2018). The simulations are on a 100 km × 100 km periodic domain for uniform sea surface temperatures set to 295 (blue), 300 (black), and 305 K (red). Updraft velocity at each level is the mean of vertical velocities w that exceed the 99.9th percentile ($w_{>99.9}$).

4. Summary and Discussion

Moist adiabatic warming varies non-monotonically with respect to surface temperature. The non-monotonicity arises because of a competition between two limiting factors of condensation: availability of water vapor and adiabatic cooling. At low surface temperatures, condensation is limited by the availability of water vapor and thus moist adiabatic warming scales like Clausius-Clapeyron while at high surface temperatures condensation is limited by adiabatic cooling. The surface temperature where moist adiabatic warming peaks approximately follows $c_L = c_{pd}$, where $c_L = L_v \partial q_s / \partial T$. The non-monotonicity of moist adiabatic warming propagates to buoyancy because buoyancy scales as the difference between an entraining lapse rate and the moist adiabatic lapse rate. The surface temperature where buoyancy peaks approximately follows $c_L = c_{pd}\sqrt{1+a}$, where a is the entrainment parameter as defined in Romps (2016). Finally the non-monotonicity of buoyancy propagates to the vertical velocity profile of convective updrafts. Cloud resolving models simulating radiative convective equilibrium exhibit diverse but qualitatively consistent responses in strong convective updrafts to surface temperature changes.

Our findings on buoyancy complement Romps (2016), who first explained the non-monotonicity of CAPE with surface temperature. He showed that CAPE peaks where $c_L = c_{pd}$. Here we derive a more general criterion for the T_s corresponding to the peak of buoyancy $c_L = c_{pd}\sqrt{1+a}$, which reduces to Romps (2016)'s criterion in the limit of zero entrainment. The factor $\sqrt{1+a}$ is insignificant in Earth's current climate (e.g. for $a = 0.2$, $\sqrt{1+a} = 1.09$) thus Romps (2016)'s criterion works well for understanding the non-monotonicity of CAPE. However, the factor $\sqrt{1+a}$ becomes important for generalizing the theory to stronger entrainment rates and for understanding the non-monotonicity of buoyancy in the lower troposphere.

The non-monotonicity of moist adiabatic warming may have additional implications for climate, such as the organization of convection and the large-scale circulation response to warming. The non-monotonicity of moist adiabatic warming would drive a non-monotonic change in the meridional and zonal temperature gradients. This could serve as a thermodynamically driven hypothesis for understanding state dependence in the response of Hadley and Walker Cells to warming.

Acknowledgments. I thank Andrew Williams, Jiawei Bao, Jonah Bloch-Johnson, Martin Singh, Stephen Po-Chedley, Nadir Jeevanjee, and two anonymous reviewers for helpful discussions and feedback on the manuscript.

Data availability statement. All scripts used for analysis and plots in this paper are available at `https://github.com/omiyawaki/miyawaki-2025-nonmonotonic-moist-adiabat`. They will also be archived on Zenodo upon publication.

APPENDIX A

Calculation of Moist Adiabatic Profiles

The moist adiabatic profiles are calculated numerically by assuming that saturation moist static energy h is conserved, where:

$$h = c_p T + gz + L_v q_s \tag{A1}$$

Here, T is temperature, z is height, q_s is the saturation specific humidity, g is the acceleration due to gravity, c_p is the specific heat of dry air at constant pressure, and L_v is the latent heat of vaporization. All thermodynamic constants are defined in Table A1. Saturation vapor pressure is calculated using Eq. (10) in Bolton (1980).

The calculation proceeds in discrete vertical steps of $\Delta p = 50$ Pa). For a given surface temperature (T_s) and surface pressure (p_s), h is first calculated at the surface ($z = 0$) and is held constant over height. At each subsequent pressure step p_{i+1}, the height z_{i+1} is calculated using hydrostatic balance. Then, a numerical root-finding algorithm (scipy.optimize.root_scalar with the Brentq method) is used to find the temperature T_{i+1} that satisfies the condition that the h at $(T_{i+1}, p_{i+1}, z_{i+1})$ is equal to the surface h.

To demonstrate that the non-monotonic warming is independent of the vertical coordinate, the results are also presented in height coordinates (Fig. A1). These profiles are obtained by following the same calculation as above except stepping in uniform intervals $\Delta z = 100$ m. The pressure p_{i+1} at height z_{i+1} is calculated using hydrostatic balance.

APPENDIX B

Effect of Latent Heat of Fusion on Moist Adiabatic Warming

We assess how latent heat of fusion influences the non-monotonicity of moist adiabatic warming. We follow the IFS Cycle 40 approximations as summarized by Flannaghan et al. (2014). The fig-a1.png

Fig. A1. The moist adiabatic warming response to a 4 K surface warming in pressure coordinates. (a) Vertical profiles of the temperature response (ΔT) as a function of pressure for surface temperatures (T_s) 280, 290, 300, 310, and 320 K. (b) The warming (ΔT) at 5 km, 10 km, 15 km, and 20 km as a function of T_s. The non-monotonic behavior seen in height coordinates (Fig. 1c) is also evident in pressure coordinates.

fraction of liquid water α varies with T as follows:

$$\alpha(T) = \begin{cases} 0, & T \leq T_{\text{ice}}, \\ \left(\dfrac{T - T_{\text{ice}}}{T_0 - T_{\text{ice}}}\right)^2 & T_{\text{ice}} < T < T_0, \\ 1 & T \geq T_0, \end{cases} \tag{B1}$$

TABLE A1. Thermodynamic constants used in the calculation of moist adiabatic profiles.

Symbol	Description	Value	Units
g	Acceleration due to gravity	9.81	m s^{-2}
c_p	Specific heat of dry air	1005.7	J kg^{-1} K^{-1}
R_d	Gas constant for dry air	287.05	J kg^{-1} K^{-1}
R_v	Gas constant for water vapor	461.5	J kg^{-1} K^{-1}
ϵ	Ratio of gas constants (R_d/R_v)	0.622	dimensionless
p_s	Surface pressure	1000	hPa
L_v	Latent heat of vaporization	2.501×10^6	J kg^{-1}

where $T_{\text{ice}} = 253.15$ K and $T_0 = 273.15$ K. Thus all condensate is ice below 253.15 K, all condensate is liquid above 273.15 K, and a quadratic transition occurs in between.

The saturation vapor pressure e_s is the weighted average over liquid (e_ℓ) and ice (e_i):

$$e_s = \alpha e_\ell + (1-\alpha)e_i \tag{B2}$$

The saturation vapor pressure over liquid and ice is:

$$e_{\ell,i}(T) = a_1 \exp\left(a_3 \frac{T-T_0}{T-a_4}\right) \tag{B3}$$

where over liquid $a_1 = 611.21$ Pa, $a_3 = 17.502$, $a_4 = 32.19$ K (Buck 1981) and over ice $a_1 = 611.21$ Pa, $a_3 = 22.587$, $a_4 = -0.7$ K (Alduchov and Eskridge 1996).

The effective latent heat of vaporization $L_e(T)$ includes both condensation and fusion:

$$L_e(T) = L_v + (1-\alpha)L_f \tag{B4}$$

where $L_f = 0.334\times10^6$ J kg^{-1} is the latent heat of fusion.

Moist adiabats are obtained by solving for T that conserves moist static energy with the effective latent heat L_e:

$$h = c_{pd}T + gz + L_e q_s \tag{B5}$$

The vertical profiles of warming ΔT and the warming at fixed pressure levels versus surface temperature exhibit similar non-monotonic behavior to the case without fusion (compare Fig. 1

and B1). Latent heat of fusion introduces a secondary local maximum in the warming in the mid troposphere (500 hPa) due to the additional energy release from fusion. When the secondary peak is to the right of the primary peak the T_s corresponding to peak warming shifts to colder T_s with fusion (points below the 1:1 line in Fig. B1). As the secondary peak overlaps with the primary peak the T_s corresponding to peak warming shifts to warmer T_s with fusion (points above the 1:1 line in Fig. B1). This effect is greatest (6.03 K) at 727 hPa. Since fusion represents a secondary effect and complicates analytical treatment, we neglect it for the rest of the paper.

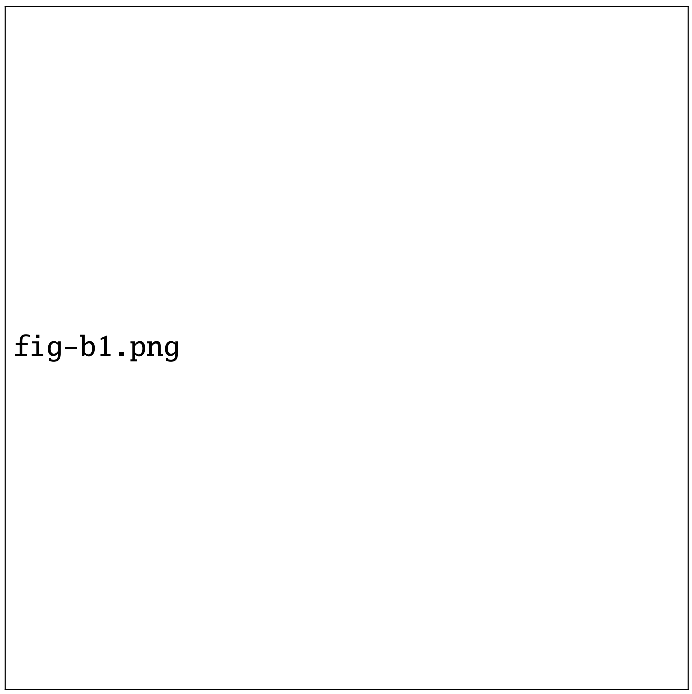

FIG. B1. The moist adiabatic warming response to a 4 K surface warming with latent heat of fusion. (a) Vertical profiles of the temperature response (ΔT) as a function of pressure for surface temperatures (T_s) of 280, 290, 300, 310, and 320 K. (b) The warming (ΔT) at fixed pressure levels of 500, 400, 300, and 200 hPa as a function of T_s. (c) T_s corresponding to peak warming with and without fusion.

APPENDIX C

Effect of Saturation Vapor Pressure Formula on Moist Adiabatic Warming

The calculation of moist adiabatic warming profiles depends on the choice of the saturation vapor pressure formula. To assess the sensitivity of surface temperatures associated with peak moist adiabatic warming to different formula we test three formula: Bolton (1980), Goff-Gratch (List 1949), and Murphy and Koop (2005).

The Bolton (1980) formula is:

$$e_s = 6.112 \exp\left(\frac{17.67(T - 273.15)}{T - 29.65}\right) \quad [\mathrm{hPa}], \tag{C1}$$

The Goff-Gratch formula is:

$$\begin{aligned}\log_{10} e_w = -7.90298\left(\frac{373.16}{T} - 1\right) + 5.02808 \log_{10}\left(\frac{373.16}{T}\right) \\ - 1.3816 \times 10^{-7}\left(10^{11.344(1-T/373.16)} - 1\right) \\ + 8.1328 \times 10^{-3}\left(10^{-3.49149(373.16/T-1)} - 1\right) \\ + \log_{10}(1013.246) \quad [\mathrm{hPa}]\end{aligned} \tag{C2}$$

The Murphy and Koop (2005) formula is:

$$\begin{aligned}\ln e_w = 54.842763 - \frac{6763.22}{T} - 4.210 \ln T + 0.000367T \\ + \tanh(0.0415(T - 218.8))\left(53.878 - \frac{1331.22}{T} - 9.44523 \ln T + 0.014025T\right) \quad [\mathrm{Pa}],\end{aligned} \tag{C3}$$

where T is in Kelvin for all 3 formula.

Bolton (1980) is sufficiently accurate for the purposes of evaluating the T_s that leads to maxima in moist adiabatic warming (Fig. C1). The differences in peak T_s across the three saturation vapor pressure formula are small, with the largest deviation being 0.27 K between Bolton and Goff-Gratch and 0.34 K between Bolton and Murphy-Koop. Thus we use Bolton (1980) for the rest of the paper.

fig-c1.png

FIG. C1. (a) T_s corresponding to peak warming using Bolton (1980) and Goff-Gratch saturation vapor pressure formula. (b) Same as (a) but comparing Bolton (1980) and Murphy and Koop (2005).

References

Alduchov, O. A., and R. Eskridge, 1996: Improved magnus form approximation of saturation vapor pressure. *Journal of Applied Meteorology*, **35 (4)**, 601–609.

Bolton, D., 1980: The computation of equivalent potential temperature. *Mon. Weather Rev.*, **108 (7)**, 1046–1053.

Buck, A. L., 1981: New equations for computing vapor pressure and enhancement factor. *Journal of Applied Meteorology and Climatology*, **20 (12)**, 1527–1532.

Del Genio, A. D., M.-S. Yao, and J. Jonas, 2007: Will moist convection be stronger in a warmer climate?: CONVECTION STRENGTH IN a WARMER CLIMATE. *Geophys. Res. Lett.*, **34 (16)**.

Emanuel, K. A., 1994: *Atmospheric Convection*. Oxford University Press.

Flannaghan, T. J., S. Fueglistaler, I. M. Held, S. Po-Chedley, B. Wyman, and M. Zhao, 2014: Tropical temperature trends in atmospheric general circulation model simulations and the impact of uncertainties in observed SSTs. *Journal of Geophysical Research, D: Atmospheres*, **119 (23)**, 13,327–13,337.

Hansen, J., A. Lacis, D. Rind, G. Russell, P. Stone, I. Fung, R. Ruedy, and J. Lerner, 1984: Climate sensitivity: Analysis of feedback mechanisms. *Climate Processes and Climate Sensitivity*, American Geophysical Union (AGU), 130–163.

Held, I. M., 1993: Large-scale dynamics and global warming. *Bull. Am. Meteorol. Soc.*, **74 (2)**, 228–242.

Held, I. M., and K. M. Shell, 2012: Using relative humidity as a state variable in climate feedback analysis. *Journal of climate*, **25 (8)**, 2578–2582.

Held, I. M., and B. J. Soden, 2000: Water vapor feedback and global warming. *Annual review of energy and the environment*, **25 (1)**, 441–475.

Levine, X. J., and W. R. Boos, 2016: A mechanism for the response of the zonally asymmetric subtropical hydrologic cycle to global warming. *J. Clim.*, **29 (21)**, 7851–7867.

List, R. J., 1949: Smithsonian meteorological tables. *Smithsonian miscellaneous collections*, **114**, 1–521.

Miyawaki, O., Z. Tan, T. A. Shaw, and M. F. Jansen, 2020: Quantifying key mechanisms that contribute to the deviation of the tropical warming profile from a moist adiabat. *Geophys. Res. Lett.*, **47 (20)**, e2020GL089 136.

Murphy, D. M., and T. Koop, 2005: Review of the vapour pressures of ice and supercooled water for atmospheric applications. *Quarterly journal of the Royal Meteorological Society. Royal Meteorological Society (Great Britain)*, **131 (608)**, 1539–1565.

Neelin, J. D., and I. M. Held, 1987: Modeling tropical convergence based on the moist static energy budget. *Mon. Weather Rev.*, **115 (1)**, 3–12.

O'Gorman, P. A., 2015: Precipitation extremes under climate change. *Current climate change reports*, **1 (2)**, 49–59.

Romps, D. M., 2016: Clausius–Clapeyron scaling of CAPE from analytical solutions to RCE. *J. Atmos. Sci.*, **73 (9)**, 3719–3737.

Santer, B. D., and Coauthors, 2005: Amplification of surface temperature trends and variability in the tropical atmosphere. *Science*, **309 (5740)**, 1551–1556.

Seeley, J. T., N. Jeevanjee, and D. M. Romps, 2019: FAT or FiTT: Are anvil clouds or the tropopause temperature invariant? *Geophysical research letters*, **46 (3)**, 1842–1850.

Vallis, G. K., P. Zurita-Gotor, C. Cairns, and J. Kidston, 2015: Response of the large-scale structure of the atmosphere to global warming. *Quart. J. Roy. Meteor. Soc.*, **141 (690)**, 1479–1501.

Wing, A. A., K. A. Reed, M. Satoh, B. Stevens, S. Bony, and T. Ohno, 2018: Radiative–convective equilibrium model intercomparison project. *Geoscientific Model Development*, **11 (2)**, 793–813.